Genetic background effects of keratin 8 and 18 in a DDC-induced hepatotoxicity and Mallory-Denk body formation mouse model

Johannes Haybaeck[1], Cornelia Stumptner[1], Andrea Thueringer[1], Thomas Kolbe[2], Thomas M Magin[3], Michael Hesse[4], Peter Fickert[5], Oleksiy Tsybrovskyy[1], Heimo Müller[1], Michael Trauner[5,6], Kurt Zatloukal[1] and Helmut Denk[1]

Keratin 8 (K8) and keratin 18 (K18) form the major hepatocyte cytoskeleton. We investigated the impact of genetic loss of either K8 or K18 on liver homeostasis under toxic stress with the hypothesis that K8 and K18 exert different functions. krt8$^{-/-}$ and krt18$^{-/-}$ mice crossed into the same 129-ola genetic background were treated by acute and chronic administration of 3,5-diethoxy-carbonyl-1,4-dihydrocollidine (DDC). In acutely DDC-intoxicated mice, macrovesicular steatosis was more pronounced in krt8$^{-/-}$ and krt18$^{-/-}$ compared with wild-type (wt) animals. Mallory-Denk bodies (MDBs) appeared in krt18$^{-/-}$ mice already at an early stage of intoxication in contrast to krt8$^{-/-}$ mice that did not display MDB formation when fed with DDC. Keratin-deficient mice displayed significantly lower numbers of apoptotic hepatocytes than wt animals. krt8$^{-/-}$, krt18$^{-/-}$ and control mice displayed comparable cell proliferation rates. Chronically DDC-intoxicated krt18$^{-/-}$ and wt mice showed a similarly increased degree of steatohepatitis with hepatocyte ballooning and MDB formation. In krt8$^{-/-}$ mice, steatosis was less, ballooning, and MDBs were absent. krt18$^{-/-}$ mice developed MDBs whereas krt8$^{-/-}$ mice on the same genetic background did not, highlighting the significance of different structural properties of keratins. They are independent of the genetic background as an intrinsic factor. By contrast, toxicity effects may depend on the genetic background. krt8$^{-/-}$ and krt18$^{-/-}$ mice on the same genetic background show similar sensitivity to DDC intoxication and almost resemble wt animals regarding survival, degree of porphyria, liver-to-body weight ratio, serum bilirubin and liver enzyme levels. This stands in contrast to previous work where krt8$^{-/-}$ and krt18$^{-/-}$ mice on different genetic backgrounds were investigated.

Laboratory Investigation (2012) 92, 857–867; doi:10.1038/labinvest.2012.49; published online 26 March 2012

KEYWORDS: DDC; intermediate filaments; keratin deficiency; sclerosing cholangitis; steatohepatitis

Keratins (Ks) form the epithelial intermediate filament (IF) cytoskeleton.[1] The analysis of K knockout and transgenic mice revealed that Ks of internal epithelia are major contributors to cell integrity.[2–5] Krt8 and Krt18 are believed to be susceptibility genes for liver disease. In the absence of Ks, overall protein biosynthesis was diminished by ~40%.[6] Lack or mutation of K8 or K18 predispose for liver injury and apoptosis. Survival of K8-deficient (krt8$^{-/-}$) rodents seems to be determined by facultative modifier genes that differ between C57Bl/6 and FVB/N mice: krt8$^{-/-}$ mice in the C57Bl/6 background showed 94% embryonic lethality associated

with placental deficiency whereas 55% of FVB/N K8$^{-/-}$ mice survived.[7] As previously shown by Hillebrandt et al,[8] FVB mice are more resistant to develop liver fibrosis than, eg, BalbC mice. This additional example identified the Hfib1 as an important locus of fibrosis susceptibility.[8]

A relevance of K sequence variants for human liver disease was substantiated by detection of K mutations in patients of different ethnic backgrounds and with various liver diseases.[9–11]

Expression of a dominant-negative mutant of human K18 in livers of transgenic mice led to chronic hepatitis with hepatocyte fragility and increased susceptibility toward acute

[1]Institute of Pathology, Medical University of Graz, Graz, Austria; [2]Biomodels Austria, University of Veterinary Medicine Vienna, Austria and IFA-Tulln, University of Natural Resources and Applied Life Sciences, Vienna, Austria; [3]Translational Centre for Regenerative Medicine Leipzig, Institute of Biology, University of Leipzig, Leipzig, Germany; [4]Division of Cell Biochemistry, Institute of Biochemistry and Molecular Biology, University of Bonn, Bonn, Germany; [5]Division of Gastroenterology and Hepatology, Department of Internal Medicine, Laboratory of Experimental and Molecular Hepatology, Medical University of Graz, Graz, Austria and [6]Division of Gastroenterology and Hepatology, Department of Medicine III, Medical University Vienna, Vienna, Austria
Correspondence: Professor J Haybaeck, MD, PhD, Institute of Pathology, Medical University of Graz, Auenbruggerplatz 25, 8036 Graz, Austria.
E-mail: johannes.haybaeck@medunigraz.at
Received 27 September 2011; revised 7 November 2011; accepted 8 November 2011

drug-induced liver injury.[12] Following administration of hepatotoxins, hyperphosphorylation of K18 on serine residues, an increased level of soluble Ks, and reorganization of the K cytoskeleton in hepatocytes occurred, suggesting that phosphorylation of Ks has a role in protecting hepatocytes against liver injury and thus serves as 'stress sensor'.[13–16] Ks 8 and 18 are involved in mediating Fas- (but not TNFα-) induced apoptosis in hepatocytes and the apoptotic program is enhanced in K-modified cells.[17,18]

Several pathologic conditions including alcoholic steatohepatitis (ASH) and non-alcoholic steatohepatitis (NASH) show a disturbed K cytoskeleton in ballooned hepatocytes with Ks and p62 as major components of cytoplasmic aggregates termed as Mallory-Denk bodies (MDBs).[12,19,20] Steatohepatitis-like liver damage with MDB formation can be induced in mice by chronic administration of the porphyrinogenic liver toxins 3,5-diethoxy-carbonyl-1,4-dihydrocollidine (DDC) and griseofulvin.[19,20] Recent studies using different mouse strains revealed that the genetic background significantly determines the liver phenotype in the DDC model which may also be relevant for the variable susceptibility of patients to steatohepatitis.[21,22] In previous studies, we observed a strikingly higher DDC toxicity with increased lethality of K8$^{-/-}$ mice upon DDC intoxication compared with wild-type (wt) and krt18$^{-/-}$ animals.[23,24] We hypothesized that K8 protects against oxidative stress, and that the genetic background determines the steatohepatitis phenotype of krt8$^{-/-}$ and krt18$^{-/-}$ mice. We posed the question whether strains rather than K affect the susceptibility toward MDB formation, steatohepatitis and sclerosing cholangitis. We aimed at dissecting the different properties of K8 and K18, and therefore had to backcross both strains to the same genetic background (129-ola) to enable a direct comparison. We therefore generated krt8$^{-/-}$ and krt18$^{-/-}$ mice in the same genetic background for direct comparison using the DDC model with special emphasis on resulting steatohepatitis and the behavior of MDBs.

MATERIALS AND METHODS
Breeding of Mice
After having performed embryo transfers heterozygous krt8$^{+/-}$ FVB/N mice were mated to 129-ola wt mice over >10 generations.[2–5] Genotypes were determined by PCR analysis of tail DNA. Following primers were used: K8-868 (5'-GGC CCT GCC CTC TAG TGT-3') and K8-1377 (5'-AGG GGT CTC ACC TTG TCA AT-3') for amplification of the wt allele (K8$^+$), K8-868 and neo-249 (5'-CCT TCC CGC TTC AGT TAC-3') for amplification of the mutated allele (K8$^-$). PCR products were separated on a 1% agarose gel in 1× TBE buffer. The expected product from mK8-868 and mK8-1377 was 529 bp, from mK8-868 and neo-249 was 700 bp. Breeding and genotyping of krt18$^{-/-}$ 129-ola mice was performed as described previously.[2–5]

Intoxication
Homozygous male krt8$^{-/-}$, krt18$^{-/-}$ and Wt 129-ola mice (2 months old, body weight 25–30 g) were kept under SPF conditions and fed a standard diet (ssniff Spezialitäten GmbH, Soest, Germany) and water ad libitum. For experimental induction of steatohepatitis, mice received standard diet containing 0.1% DDC (Aldrich, Steinheim, Germany) for 1 and 12 weeks, respectively. At each time point and in each experimental group, 5–10 mice were killed by cervical dislocation, body and liver weights were determined, serum samples were analyzed, and the livers were further processed as indicated below. All experiments were approved and conform to the guidelines of the Austrian Animal Protection Law, Veterinary office, Vienna, Austria. The experimental protocol was approved by the Federal Animal Care and Use Committee.

Light Microscopy
Murine liver tissues were either snap frozen in methylbutane precooled in liquid nitrogen or fixed in 4% formaldehyde solution in PBS, embedded in paraffin, and 7 μm thick sections were cut and subsequently stained with hematoxylin and eosin (HE) or Sirius red, respectively. Apoptotic hepatocytes were determined by their morphological features of showing eosinophilic cytoplasms and shrunken nuclei.

Immunofluorescence Microscopy
Murine liver tissues were snap frozen in methylbutane precooled in liquid nitrogen for immunofluorescence microscopy, which was performed as described previously.[23,25,26] Apoptosis was detected by immunofluorescence microscopy on cryosections fixed with acetone using a polyclonal antibody against activated caspase 3 and a rhodamin-conjugated secondary antibody. For quantitative determination, positive hepatocytes were counted in 20–40 microscopic fields (×250 magnification).

Immunohistochemistry
Murine liver tissues were fixed in 4% formaldehyde solution in PBS, embedded in paraffin, and 7 μm thick sections were cut and subsequently used for immunohistochemistry, was performed as described.[19,20,23,25,26] For determination of the proliferation status, Ki-67$^+$ and PCNA$^+$ hepatocyte nuclei were counted in 10 high power fields (HPF; ×400 magnification) and mean values (± s.d.) were calculated.

Immunoelectron Microscopy
Immunoelectron microscopy was performed for MDB characterization as described previously.[23,25,26]

Bile Duct/Ductule Morphometry
Morphometry of osteopontin (OPN) expression in bile ducts and ductules was performed using a semiautomatic system for image analysis. This consisted of a microscope (Nikon E600; Tokyo, Japan), a video camera (Sony DXC-930P;

Tokyo, Japan), a frame grabber (Intrigue Pro; Integral Technologies, Indianapolis, IN), and a computer with image analysis software (Optimas 6.51; Media Cybernetics, Bethesda, MD). A macro-command served for automatic identification and measurement of the total area of OPN$^+$ cells within a given portal field. All portal fields (13–31) in each sample were measured.

Porphyrin Determination
Total porphyrin content was determined as described previously.[23] Brown pigment in liver tissue of intoxicated mice indicating porphyrin deposition was quantified morphometrically by evaluating 38–134 randomly selected HPF.

Immunoblotting
K8 and K18 proteins were analyzed in liver homogenates of control, 1 and 12 weeks DDC-fed wt and krt8$^{-/-}$ mice by immunoblotting using rabbit antibody 50K160 directed to both Ks.[27]

Quantitative Real-Time PCR
Routine protocols were performed. Primers and probes (synthesized by MWG-Biotech AG, Germany) are listed in Table 1.

Statistical Analysis
Data are reported as median values with 95% confidence interval limits. These estimates were computed by non-parametric bootstrap using DATAPLOT software (National Institute of Standards and Technology, Statistical Engineering Division, Gaithersburg, MD, USA). Morphometric data present a hierarchical structure, where portal fields or fields of view (level-one sampling units) are nested within mice (level-two sampling units). A two-level linear regression model by means of MLwiN 2.02 software (Centre for Multilevel Modelling, University of Bristol, UK) was fitted to calculate mean values and confidence intervals. Finally, a two-way ANOVA with Bonferroni post-test was performed to test the significance of differences between groups.

RESULTS
Effect of DDC Intoxication on Liver Weight, Serum Bilirubin and Hepatic Porphyrin Levels are Independent of the Keratin Status, While Transaminase Levels and Ductular Reaction Are Aggravated in krt18$^{-/-}$ Mice
The livers of DDC-fed (treatment for 1 and 12 weeks, respectively) compared with normal diet-fed wt, krt8$^{-/-}$ and krt18$^{-/-}$ mice were markedly enlarged. Liver-to-body weight ratios did not differ between wt and K-deficient mice on normal control diet ($P > 0.05$; Figure 1a). DDC intoxication led to similar significant increase of liver-to-body weight ratios in all groups (***, $P < 0.0001$; Figure 1a). Serum bilirubin levels rose with duration of DDC intoxication equally in wt and K-deficient mice (**, $P = 0.004$; Figure 1b). In control diet-fed mice, K deletion had no influence on distribution and quantity of bile ducts and ductules. DDC treatment for 1 week led to ductular reaction without significant difference between the experimental groups. Bile duct areas increased in chronically DDC-intoxicated mice (***, $P < 0.0001$). However, ductular reaction was significantly more pronounced in krt8$^{-/-}$ and krt18$^{-/-}$ mice when compared with DDC-intoxicated wt mice (*, $P = 0.02$ or $P < 0.05$, respectively; Figure 1c).

Alkaline phosphatase (ALP) levels rose equally in acutely and chronically intoxicated animals (Figure 1d). Serum aminotransferase (AST, ALT) levels peaked after short-term intoxication and dropped in the chronic stage (Figures 1e and f). In 1-week DDC-treated mice, AST levels were significantly higher in krt18$^{-/-}$ mice compared with wt (***, $P < 0.0001$), while in krt8$^{-/-}$ they did not significantly differ from wt mice (Figure 1e).

Activated caspase 3$^+$ hepatocytes were sparse in all groups, which were fed with normal diet. Upon DDC treatment for 1 week significantly increased numbers of hepatocytes with caspase 3 activation were found in wt as well as in K-deficient mice with significant difference between wt and krt8$^{-/-}$ or krt18$^{-/-}$ mice (*, $P = 0.02$; Figure 2a). Upon challenge with DDC for 12 weeks, the K-deficient groups showed a significantly lower number of hepatocytes with caspase 3 activation in

Table 1 Primer sequences for quantitative real time PCRs.

| Gene	Acc. no.	Primer/probe (dye label)	Sequence 5′–3′	Product length
p62	NM_011018	Forward primer	ACCCACAGGGCTGAAGGAAGCT	124 bp
		Reverse primer	TGGTGAGCCAGCCGCCTTCAT	(Pos 1282–1158)
Hmox 1	NM_010442	Forward primer	CACTTCGTCAGAGGCCTGCTA	93 bp
		Reverse primer	GTCTGGGATGAGCTAGTGCTGAT	(Pos 925–832)
Tbp	NM_013684	Forward primer	CGGTAGCGGTGGCGGGTATC	74 bp
		Reverse primer	CTGGGCACTGCGGAGAAAATGAC	(Pos 115–41)
mK8	NM_031170	Forward primer	TGAACAACAAGTTCGCCTCCTT	109 bp
		Reverse primer	GCTCCTCGACGTCTTCTGCT	(Pos 523–414)
mK18	NM_010664	Forward primer	GGCTCAGATCCTTGCGAATTC	84 bp
		Reverse primer	TCTAAAGTCATCGGCGGCA	(Pos 5128–444)
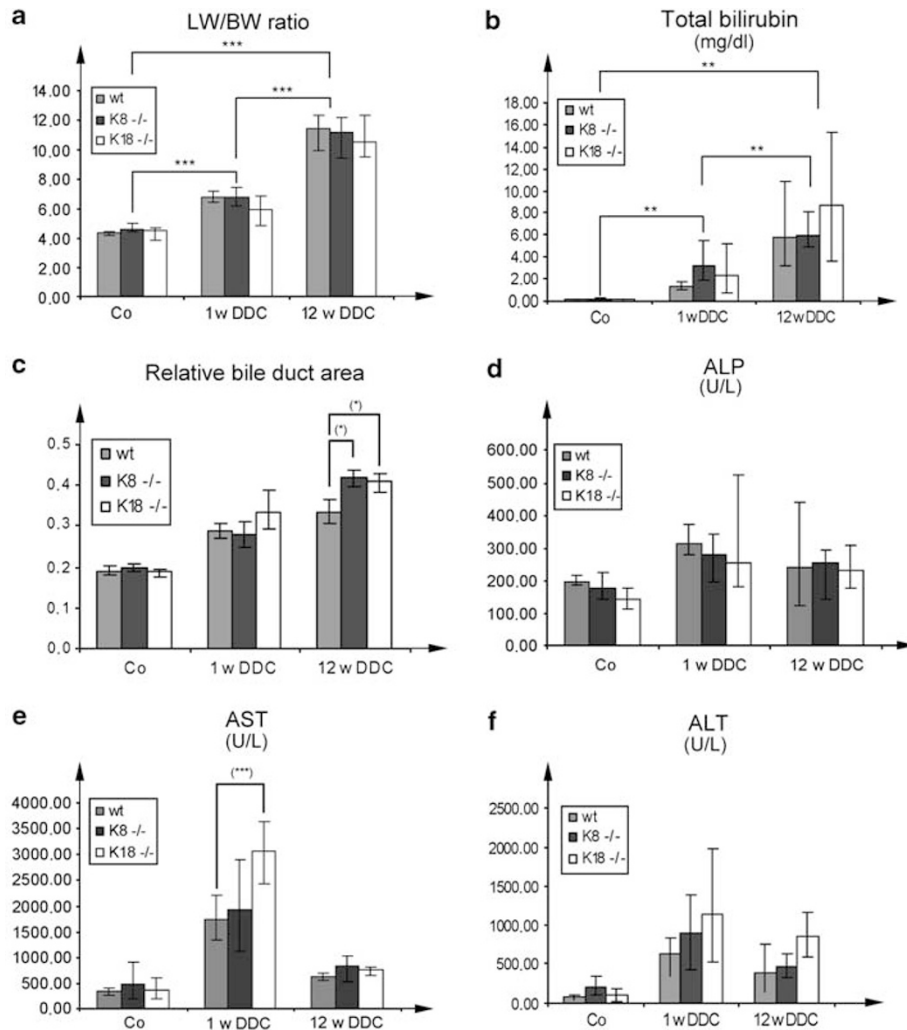
Figure 1 Liver-to-body weight ratios (LW/BW ratio), total bilirubin, serum enzyme levels (alkaline phosphatase, ALP; aspartate aminotransferase, AST; alanine aminotransferase, ALT) and relative bile duct areas in control (Co), 1 week (1w DDC) and 12 weeks (12w DDC) intoxicated wild-type (wt), K8 (krt8$^{-/-}$)- and K18 (krt18$^{-/-}$)-deficient mice. (**a**) LW/BW ratio: significant increase ($P < 0.05$) in all experimental groups. (**b**) Total bilirubin: significant increase ($P < 0.05$) in all experimental groups. (**c**) Relative bile duct area: significant difference between 12w DDC K-deficient and 12w DDC wt mice ($P < 0.05$). (**d**) ALP: no significant differences. (**e**) AST: significant difference between 1w DDC krt18$^{-/-}$ and 1w DDC wt mice ($P < 0.05$) and between all 1w DDC and all 12w DDC mice ($P < 0.05$). (**f**) ALT: no significant differences.
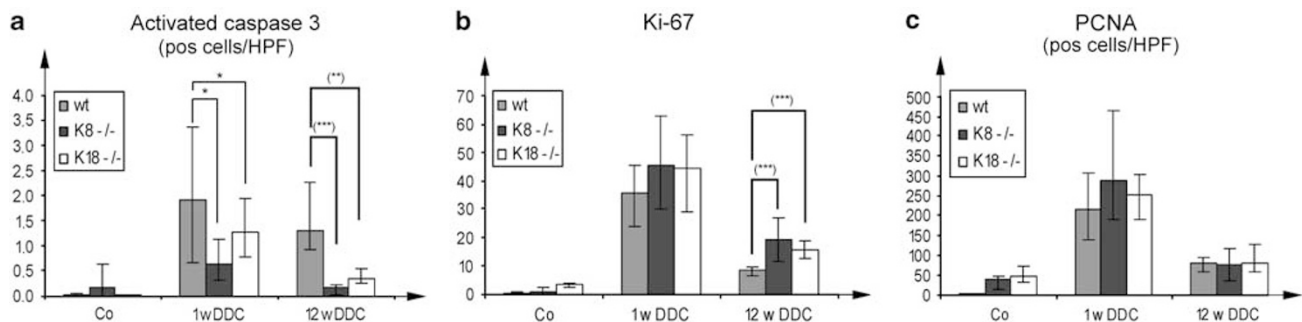

Figure 2 (**a**) Activated caspase 3: significant difference between 12w DDC K-deficient and 12w DDC wt mice ($P < 0.05$). (**b**) Ki-67: significant difference between all DDC-treated and control mice and between 12w DDC K-deficient and wt mice ($P < 0.05$). (**c**) PCNA: significant difference between all 1w DDC and control mice and between all 1w DDC and all 12w DDC mice ($P < 0.05$).

comparison with wt animals. The decrease was more pronounced in krt8$^{-/-}$ (***, $P < 0.0001$) than in krt18$^{-/-}$ animals (**, $P = 0.002$; Figure 2a).

In contrast to wt animals, in 1-week DDC-fed krt8$^{-/-}$ and krt18$^{-/-}$ mice a slight but not significant increase of Ki-67$^+$ and PCNA$^+$ nuclei was noted (Figures 2b and c). Upon long-term intoxication, cell proliferation was significantly lower compared with short-term intoxication but still higher than in the animals fed control diet. krt8$^{-/-}$ and krt18$^{-/-}$ mice significantly exceeded wt mice in this regard (***, $P < 0.0001$; Figures 2b and c). These findings suggest that lack of K causes more hepatocellular injury with a higher cellular turnover, independent of a higher susceptibility toward apoptosis. Confluent necrosis, morphologically resembling bile infarcts, was occasionally seen in acinar zone 1 (data not shown). Necrotic hepatocytes surrounded and penetrated by neutrophils were disseminated throughout the hepatic lobules in K8$^{-/-}$ and K18$^{-/-}$ mice. Interestingly, the sensitivity of transaminase levels for measuring cell death seems to be low while it is high for detection of cell turnover in this model.

DDC feeding resulted in protoporphyria in all experimental groups and liver porphyrin content significantly increased with duration of treatment (**, $P < 0.002$; Figures 3a and b). Liver porphyrin content was slightly higher, although variable, in the krt8$^{-/-}$ group. These findings agreed with morphometrically assessed hepatic pigment deposition (Figures 3a–c). After 12 weeks of DDC feeding, the accumulation of pigment was significantly higher than after 1 week of DDC treatment (*, $P = 0.03$; Figure 3c). Therefore, DDC-induced porphyria is independent of the K status.

Liver Morphology of wt, krt8$^{-/-}$ and krt18$^{-/-}$ Mice Differs upon Feeding with Normal Diet and DDC for 1 or 12 Weeks

Wt mice on control diet displayed normal liver morphology. A very mild predominantly macrovesicular steatosis without zonal predominance was observed in wt mice upon 1-week DDC feeding.

In addition to porphyria with pigment-containing macrophages and ductular reaction induced by DDC feeding, morphological features similar to human steatohepatitis were present. The latter were scored according to Brunt (NAS score).[28] Wt and krt$^{-/-}$ hepatocytes showed microvesicular and macrovesicular steatosis, and steatosis was more pronounced in krt8$^{-/-}$ than in wt mice.

No significant difference in the activity (and fibrosis) scores was observed between krt18$^{-/-}$ and wt mice ($P > 0.05$). Activity scores in krt8$^{-/-}$ mouse livers were significantly lower than in wt mice (*, $P = 0.002$), particularly due to less pronounced ballooning (Figure 3d).

Confluent necroses, morphologically resembling bile infarcts, were occasionally seen in acinar zone 1 in all animals investigated (data not shown). Upon DDC treatment for 12 weeks, wt and K-deficient mice displayed sclerosing cholangitis with pigment-containing interlobular bile ducts,

ductules and pronounced ductular reaction. Inflamed bile ducts were surrounded by fibroblasts. The liver parenchyma showed conspicuous anisocytosis, apoptotic bodies, ballooning and MDB formation in wt mice.

krt8$^{-/-}$ and krt18$^{-/-}$ mouse livers revealed disseminated but predominantly subcapsular hemorrhagic parenchymal necrosis, disseminated erythrocyte-containing hepatocytes and parenchymal areas with syncytial changes of the latter as described previously (Figure 3e).[29] Necrotic hepatocytes surrounded and penetrated by neutrophils were disseminated throughout the hepatic lobules in krt8$^{-/-}$ and krt18$^{-/-}$ mice.

K8 but not K18 Is Essential for MDB Formation

Upon DDC feeding in wt mice, keratin antibodies were used to stain the IF cytoskeleton network in hepatocytes. Hepatocytes of K-deficient mice lacked K-IF staining (Figure 4a). In DDC-fed wt mice, p62 antibodies revealed small granules present in few disseminated hepatocytes or small clusters of hepatocytes with enlarged nuclei predominantly in periportal areas. Only few of these cells contained larger cytoplasmic p62$^+$ clumps. This was also observed in livers of krt8$^{-/-}$ and krt18$^{-/-}$ mice (Figures 4a and b). In krt8$^{-/-}$ mice, MDBs were absent while in krt18$^{-/-}$ mice numerous p62$^+$ MDBs (indicated by their K8, p62 and ubiquitin content) were found (Figures 4a and b).

In krt8$^{-/-}$ mice, medium-sized granules, positive for p62, in few disseminated hepatocytes were also stainable for ubiquitin (data not shown). In wt mice, K antibodies revealed increased K-IF density in enlarged hepatocytes. In krt18$^{-/-}$ mice, numerous K$^+$ cytoplasmic granules (also p62$^+$ and ubiquitin$^+$), resembling early stages of MDBs, but also typical larger MDBs were present in hepatocytes lacking K-IF (Figures 4a and b). In krt8$^{-/-}$ mice, no K$^+$ hepatocytes but K$^+$ bile duct epithelial cells were detectable. These data suggest that K8 and K18 fulfill different roles in MDB formation, as K8 but not K18 are essential for MDB formation.

Ultrastructure of MDBs in wt and krt18$^{-/-}$ Mice

Ultrastructurally MDBs of krt18$^{-/-}$ mice consisted of an irregular meshwork of short filamentous rods. Compared with MDBs in wt mice, the filaments were identical in size but less tightly packed (Figure 4c).

OPN in Livers of wt, krt8$^{-/-}$ and krt18$^{-/-}$ Mice Treated for 1 or 12 Weeks with DDC

Since OPN is upregulated in patients with steatohepatitis and sclerosing cholangitis and correlates with fibrosis, we also explored a potential relationship between OPN and Ks in our model.[30–33] OPN immunostaining was positive in acinar zone 1 hepatocytes in 1-week DDC-fed wt and K-deficient mice (Supplementary Figure 1). This expression pattern got lost upon chronic intoxication corroborating previous findings of decreased hepatic opn mRNA expression under this condition.[34] In contrast, all DDC-challenged groups displayed strong granular cytoplasmic staining in bile duct and ductular epithelia (Supplementary Figure 1). Investigation of
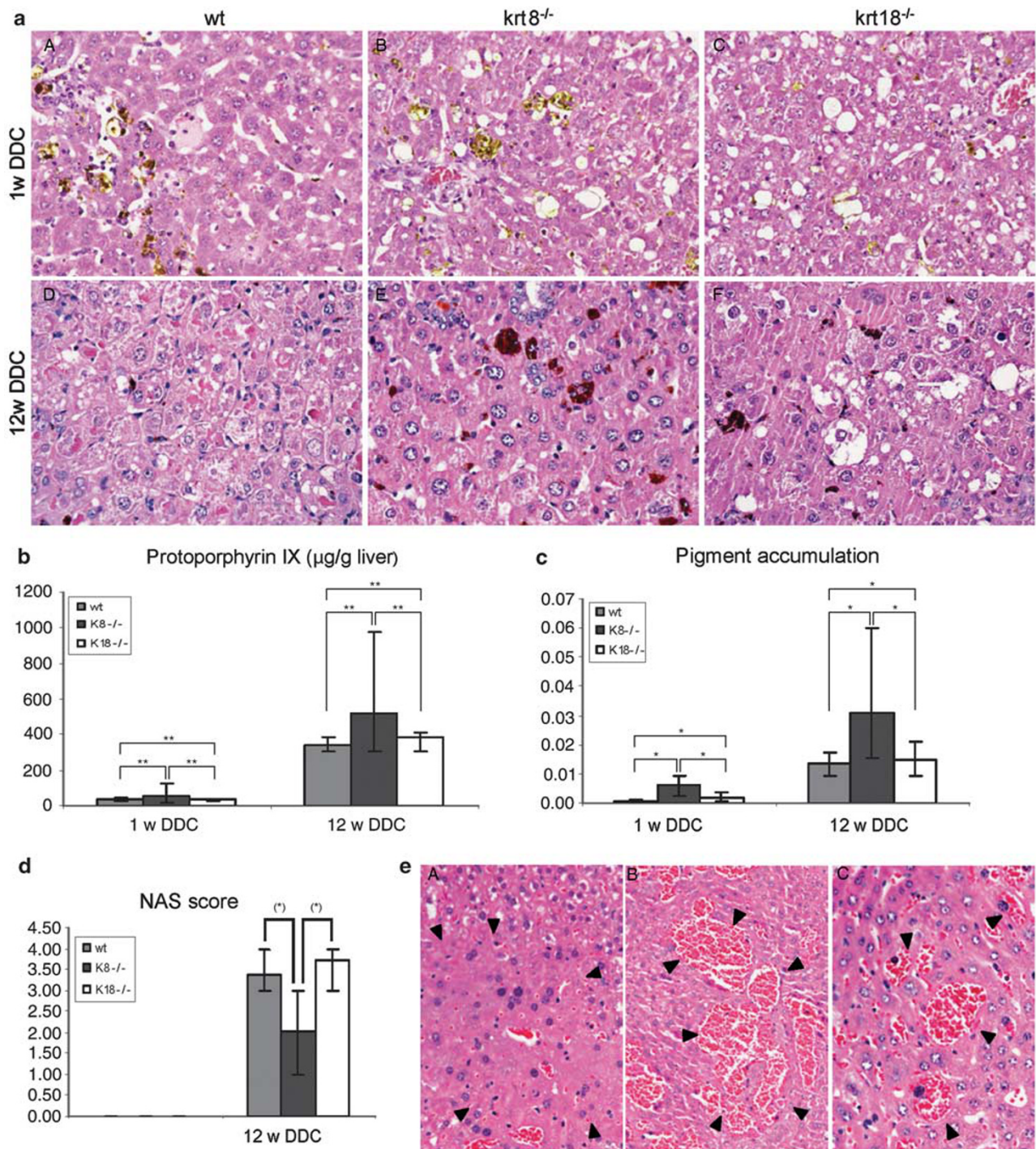
Figure 3 Steatohepatitis and protoporphyria in DDC-intoxicated wt and K-deficient mice. (**a**) After 1 week of DDC treatment (1w DDC), steatosis is more pronounced in krt8$^{-/-}$ and krt18$^{-/-}$ than in wt livers (compare A with B and C). Chronic DDC intoxication (12w DDC) is associated with hepatocyte ballooning, steatosis (and MDB formation, not clearly visible in this figure) in wt and krt18$^{-/-}$ livers (D and F). krt8$^{-/-}$ liver (E) shows less steatosis and lack ballooning and MDB formation (compare E with D and F). Protoporphyrin IX concentration (**b**) and pigment accumulation (**c**) are most conspicuous in livers of chronically (12w DDC) intoxicated mice. Liver protoporphyrin concentration is higher and pigment deposition more pronounced in krt8$^{-/-}$ than in wt and K18$^{-/-}$ mouse livers. However, due to considerable variation between animals the difference is not statistically significant. (**d**) NASH activity score (NAS score) after DDC intoxication for 12 weeks (12w DDC) is significantly lower in krt8$^{-/-}$ than in wt and krt18$^{-/-}$ mouse livers ($P < 0.05$). (**e**) Liver of krt18$^{-/-}$ mouse on control diet with parenchymal syncytial areas (A, delineated by arrowheads), extensive hemorrhagic necrosis (B, delineated by arrowheads) and hepatocytes containing erythrocytes (C, arrowheads); H-E staining.
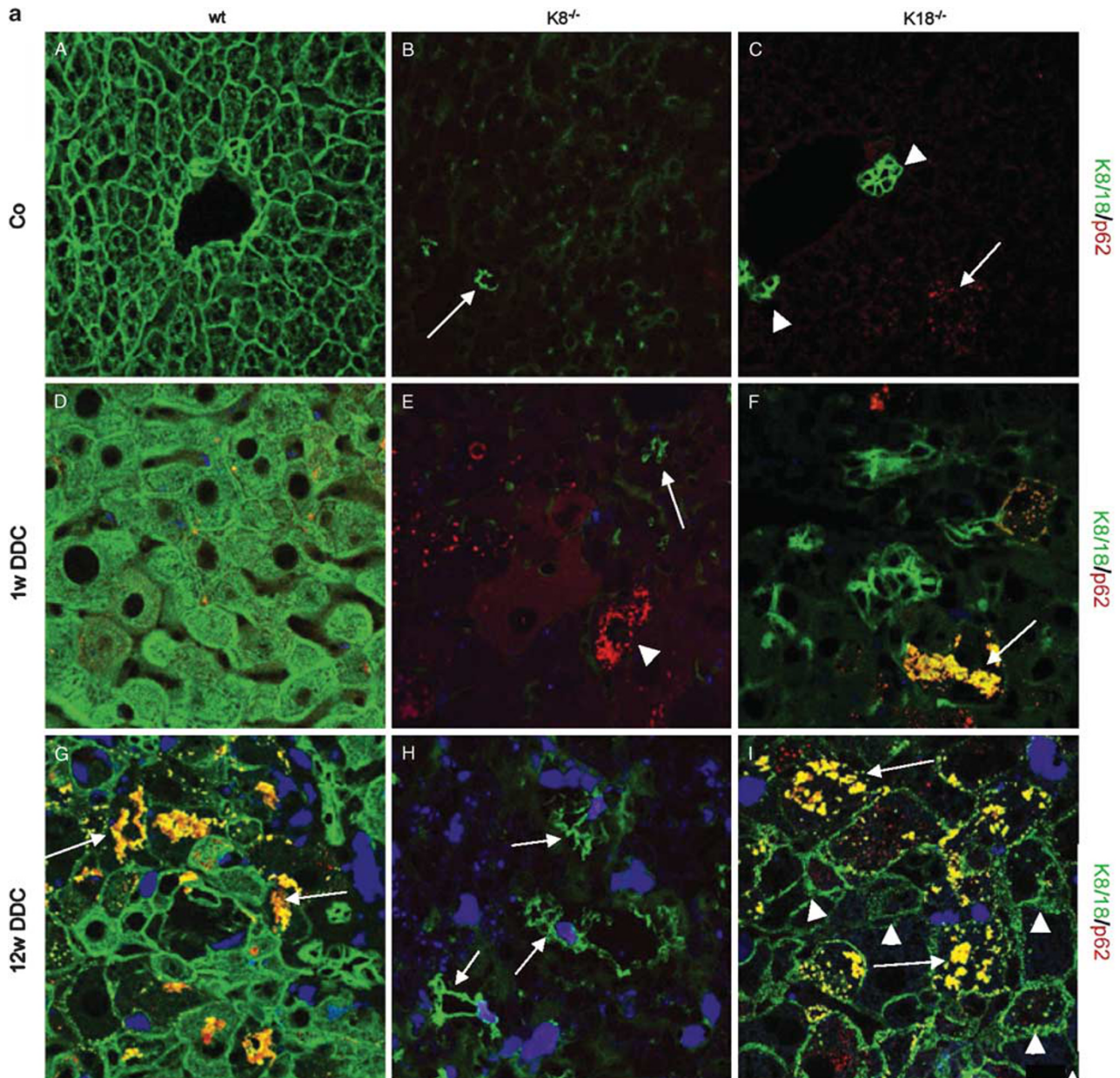
Figure 4 Double immunofluorescence microscopy, immunoelectron microscopy (IEM) of Ks in wt and K-deficient mouse livers. (**a**) K and p62 in DDC-intoxicated wt and K-deficient mice detected by double immunofluorescence microscopy against Ks 8 and 18 (K8/18; green) and p62 (red). Colocalization of the antigens is indicated by yellow color. The wt control mouse liver (Co) shows regular K-IF cytoskeleton network without p62 accumulation (A). DDC intoxication for 1 week (1w DDC) leads to enlargement of hepatocytes and increased density of the IF cytoskeleton (D). Chronic DDC intoxication (12w DDC) produces profound parenchymal damage with hepatocyte ballooning, diminution or even disappearance of the IF cytoskeleton and granular and larger MDBs (arrows in G). In K8$^{-/-}$ mice on normal diet (Co), hepatocytes are unstained by K (K) 8/18 and p62 antibodies. Only lumen-oriented linear cytoplasmic K staining of cholangiocytes is present (B; arrow). In short-term (1w DDC) DDC-intoxicated mice in addition to a superficial linear K18 staining of cholangiocytes (arrow), granular p62 is deposited in disseminated hepatocytes (E; arrowhead). In 12w DDC-intoxicated mouse livers, MDBs are absent and only the K18-related immunostaining of cholangiocytes remains (H; arrows). In krt18$^{-/-}$ mice, only cholangiocytes retain K cytoplasmic staining (arrowheads in C). Occasional hepatocytes contain p62 granules (C; arrow). In 1w DDC-intoxicated mice, MDBs are already present (F; arrow). Some hepatocytes also contain p62 in granular form. Cholangiocytes display cytoplasmic K8 immunostaining (arrowheads). Long-term DDC-intoxicated krt18$^{-/-}$ livers (12w DDC) resemble wt mice with respect to MDB formation (arrows). K8 immunostaining is retained at the periphery of some hepatocytes (arrow heads in I). p62 granules not associated with Ks are also seen (red in I). Porphyrin pigment is depicted in blue (eg, H and I). (**b**) K8, p62 and ubiquitin immunohistochemistry in DDC-fed krt18$^{-/-}$ mice. (**c**) IEM of MDBs induced by 12w DDC feeding in wt type (A and C) and krt18$^{-/-}$ (B and D) mice. The K8 immunoreaction is indicated by 18 nm gold particles, presence of p62 by 10 nm gold particles. In the wt setting, MDBs are closely associated with bundles of IF (indicated in A by arrowheads) in the krt18$^{-/-}$ situation IF are lacking. Labeling with gold particles of different sizes indicating the presence of K8 and p62 is highlighted at higher magnification in (C) and (D). Bars represent 1.5 μm (B) and 240 nm (D), respectively.

b

K8 — p62 — Ubi

c

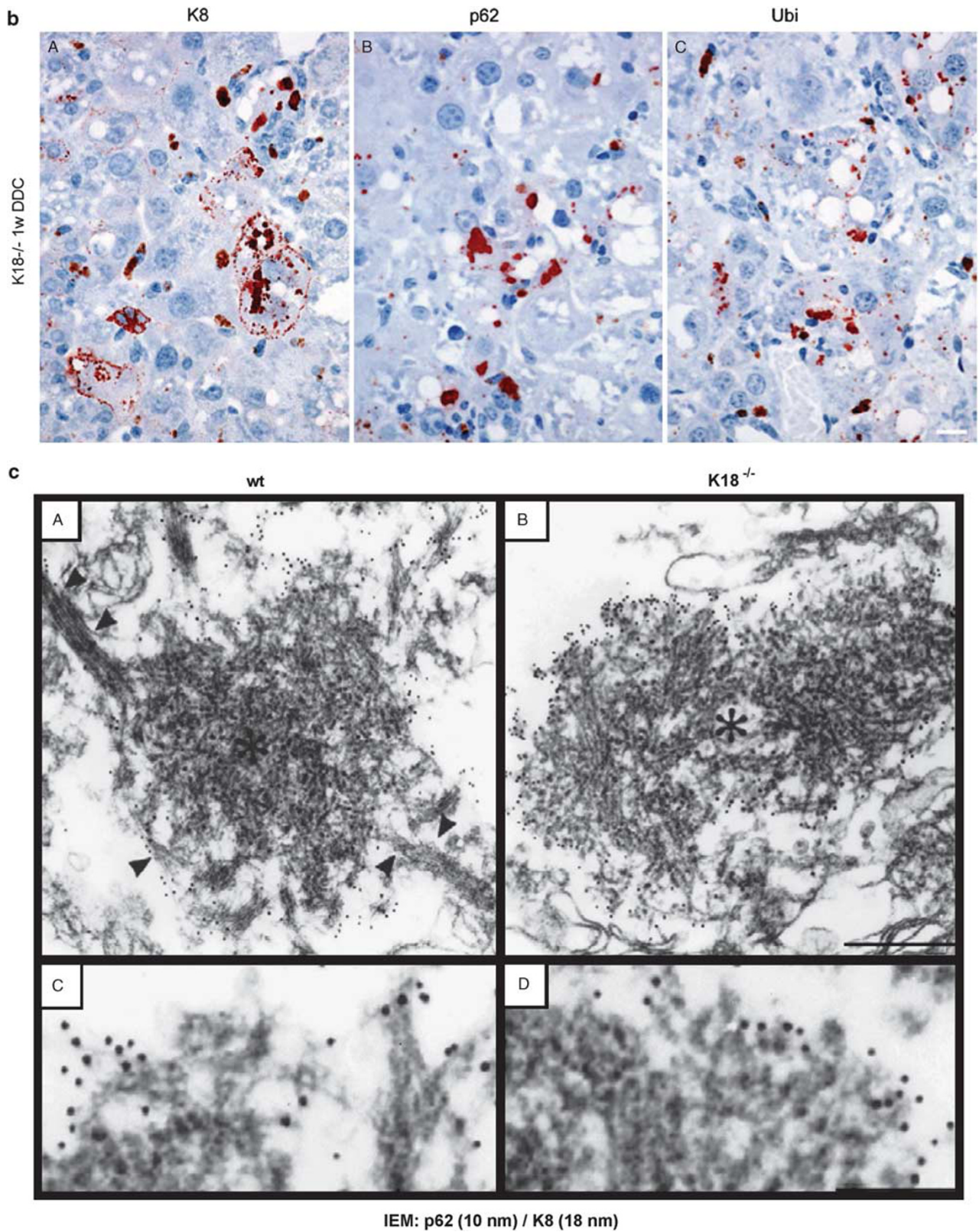wt — K18 $^{-/-}$

IEM: p62 (10 nm) / K8 (18 nm)

Figure 4 Continued.

OPN could therefore reconfirm a steatohepatitis and sclerosing cholangitis phenotype driven by DDC.

Effects of DDC Intoxication on Keratin Protein and mRNA Expression

Upon DDC intoxication for 1 week, Ks 8 and 18 were overexpressed on mRNA and protein level in wt mice (Supplementary Figures 2a–c). Chronic DDC intoxication was also associated with an increase of Ks 8 and 18 mRNA in wt livers, although less pronounced than in the acutely intoxicated animals, while K8 mRNA remained undetectable in krt8$^{-/-}$, and so was K18 mRNA in krt18$^{-/-}$ livers. In krt18$^{-/-}$ liver, K8 mRNA increased to a similar extent, whereas in the krt8$^{-/-}$ setting, the increase in K18 mRNA was significantly less (Supplementary Figure 2c). Western blot analysis of liver homogenates from chronically intoxicated krt18$^{-/-}$ mice revealed a K8-specific signal despite the absence of its type I partner under this condition (Supplementary Figure 2a), as corroborated by immunofluorescence microscopy (Supplementary Figure 2b).

DISCUSSION

In earlier studies, we found increased sensitivity of krt8$^{-/-}$ FVB/N mice to DDC intoxication as indicated by higher lethality and development of more severe protoporphiria.[23] These studies were later extended by including krt18$^{-/-}$ animals although with different (ie, 129-ola) genetic background.[26] Surprisingly, in these mice, krt18 deficiency did not cause increased sensitivity to DDC intoxication. This indicates that strain differences have a facultative modifying effect on the role of K in response to intoxication.[23]

However, the present study uncovered differences between control and K-deficient mice of the same genetic background (129-ola) and between krt8$^{-/-}$ and krt18$^{-/-}$ mice with respect to hepatotoxicity and MDB formation.

The early appearance of DDC-induced MDBs in krt18$^{-/-}$ mice supports previous findings indicating the importance of excess of K8 resulting in imbalance of the K8-to-K18 ratio for MDB formation. The key role of K8 for MDB formation is also supported by spontaneous development of MDBs in old K18$^{-/-}$ mice and in mice engineered to overexpress K8, the absence of MDBs in DDC-intoxicated krt8$^{-/-}$ mice and inhibition of MDB formation by overexpression of K18.[35–37] However, excess K8 alone is not sufficient to cause MDB formation, as revealed by acutely DDC-intoxicated wt mice that have sufficient K8. Recent work by our group uncovered molecular and cellular properties of MDB components by using polyelectrolyte probes as new diagnostic tool. In this study, we found out that cross β-sheet conformation of MDBs depends on oxidative stress and K8 but not on p62.[38] Luminescent-conjugated oligothiophenes (LCOs), h-HTAA and p-FTAA are fluorescent amyloid ligands specifically binding proteins with cross β-sheet conformation. We used LCOs to investigate conformational changes in MDBs in situ in human and murine livers as well as in transfection studies.

In conclusion, the readiness of K8 to undergo conformational changes from predominantly α-helical to cross β-sheet explains its essential role in MDB formation. This could also be a molecular structural explanation why the absence of K8 prevents MDB formation while its excess facilitates MDB formation.

The different behavior of K8 and K18 could be explained by the fact that as recently shown by Herrmann and coworkers (personal communication) by an analytical ultracentrifugation approach K18 normally exists as monomer while K8 is a mixture of various polymers. These data underline the significant contribution of IFs to protein aggregation disorders and diseases, which still have to be elucidated in further studies.

MDB generation clearly requires additional stimuli like oxidative stress leading to overexpression of the stress protein p62,[39] and eventually transglutaminase-induced crosslinking, as shown in vitro with cells transfected with major MDB components and in other studies.[25,40,41] In this context, p62 may have a dualistic role by aggregating abnormal ubiquitinated proteins but also by shuttling them to the proteasomal and/or autophagosomal machineries.[39,42] The role of impaired K-related proteolysis in MDB formation is supported by our immunoblotting and immunofluorescence data showing persistence of K8 in hepatocytes of chronically intoxicated krt18$^{-/-}$ mouse livers (Supplementary Figure 2).

The decreased apoptosis rate in krt8$^{-/-}$ and krt18$^{-/-}$ mice, particularly in the state of chronic intoxication (see also Zatloukal et al[23]), was unexpected as Ks protect hepatocytes against Fas-induced apoptosis.[43] Since p62 has a complex role in apoptosis induction and cell survival pronounced accumulation and aggregation of this protein may be critical in DDC intoxication. In any case, apoptosis does not seem to have a major role in hepatocyte disposal in the DDC model in contrast to human steatohepatitis, in which apoptosis significantly contributes to hepatocyte loss.[44]

Since krt mutations predispose to end-stage liver disease we examined the impact of Ks on DDC-induced biliary fibrosis and sclerosing cholangitis.[10,11,44] Based on our results, we conclude that the K status has no influence on the complex biliary pathology associated with DDC intoxication.

OPN has recently been described as being induced by hedgehog (Hh) signaling, and to promote fibrogenesis in NASH-related cirrhosis.[45] As in 1-week DDC-treated mice OPN$^+$ granules appear in zone 1 hepatocytes further studies on the relationship between keratin integrity and Hh signaling in acute liver toxicity will be needed. However, as in chronically DDC-intoxicated animals OPN$^+$ hepatocytes decrease in number or even disappear irrespective of the K status chronically induced K alterations do not seem to be linked to OPN.

Ductular reaction is a prominent feature of prolonged DDC intoxication and even more pronounced in intoxicated K-deficient mice. Ductular proliferation may represent a sign of parenchymal regeneration following injury, and may also be triggered by incomplete mechanical biliary obstruction.[46]

In the DDC model, both possibilities exist resulting from a combination of parenchymal damage and mechanical cholestasis.[47] Further studies are needed to clarify the question how relevant our findings are in the context of human steatohepatitis.

Based on our data and results from other groups, multiple genetic backgrounds should be investigated to understand keratin biology and its disease relevance as obviously for different functional aspects various genetic backgrounds lead to different degrees of susceptibility. Therefore, the direct comparison with human liver specimens can be clearly seen as gold standard. However, as model systems mice are highly representative as demonstrated in many publications on IFs.

In summary, krt8$^{-/-}$ and krt18$^{-/-}$ mice on the same genetic background show similar sensitivity to DDC intoxication and almost resemble wt animals regarding survival, degree of porphyria, liver-to-body weight ratios, serum bilirubin and liver enzyme levels. This stands in contrast to previous work where krt8$^{-/-}$ and krt18$^{-/-}$ mice on different genetic backgrounds were analyzed. However, our key finding was that upon DDC feeding krt18$^{-/-}$ mice developed MDBs while krt8$^{-/-}$ mice did not, suggesting that there are key differences in keratin intrinsic properties. We here demonstrate that the structural properties of K8 and K18 are genetic modifiers, which are independent of genetic background effects while toxicity effects depend on the genetic background.

DISCLOSURE/CONFLICT OF INTEREST
The authors declare no conflict of interest.

Author contributions
JH and PF contributed to concept, experimentation, data analysis and manuscript writing; CS contributed to experimentation, data analysis and manuscript writing; AT contributed to experimentation, immunofluorescence of tissues and data analysis; TMM and MT contributed to concept, data analysis and manuscript writing; TK, MH and OT contributed to experimentation and data analysis; HM performed statistical analysis; KZ and HD contributed to concept, funding, experimentation, data analysis and manuscript writing.

1. Herrmann H, Bar H, Kreplak L, et al. Intermediate filaments: from cell architecture to nanomechanics. Nat Rev Mol Cell Biol 2007;8:562–573.
2. Magin TM, Vijayaraj P, Leube RE. Structural and regulatory functions of keratins. Exp Cell Res 2007;313:2021–2032.
3. Hesse M, Grund C, Herrmann H, et al. A mutation of keratin 18 within the coil 1A consensus motif causes widespread keratin aggregation but cell type-restricted lethality in mice. Exp Cell Res 2007;313:3127–3140.
4. Coulombe PA, Wong P. Cytoplasmic intermediate filaments revealed as dynamic and multipurpose scaffolds. Nat Cell Biol 2004;6:699–706.
5. Baribault H, Price J, Miyai K, et al. Mid-gestational lethality in mice lacking keratin 8. Genes Dev 1993;7:1191–1202.
6. Vijayaraj P, Kroger C, Reuter U, et al. Keratins regulate protein biosynthesis through localization of GLUT1 and -3 upstream of AMP kinase and Raptor. J Cell Biol 2009;187:175–184.
7. Tamai Y, Ishikawa T, Bosl MR, et al. Cytokeratins 8 and 19 in the mouse placental development. J Cell Biol 2000;151:563–572.
8. Hillebrandt S, Goos C, Matern S, et al. Genome-wide analysis of hepatic fibrosis in inbred mice identifies the susceptibility locus Hfib1 on chromosome 15. Gastroenterology 2002;123:2041–2051.
9. Omary MB, Ku NO, Toivola DM. Keratins: guardians of the liver. Hepatology 2002;35:251–257.
10. Ku NO, Lim JK, Krams SM, et al. Keratins as susceptibility genes for end-stage liver disease. Gastroenterology 2005;129:885–893.
11. Ku NO, Strnad P, Zhong BH, et al. Keratins let liver live: mutations predispose to liver disease and crosslinking generates Mallory-Denk bodies. Hepatology 2007;46:1639–1649.
12. Strnad P, Stumptner C, Zatloukal K, et al. Intermediate filament cytoskeleton of the liver in health and disease. Histochem Cell Biol 2008;129:735–749.
13. Stumptner C, Omary MB, Fickert P, et al. Hepatocyte cytokeratins are hyperphosphorylated at multiple sites in human alcoholic hepatitis and in a Mallory body mouse model. Am J Pathol 2000;156:77–90.
14. Toivola DM, Ku NO, Resurreccion EZ, et al. Keratin 8 and 18 hyperphosphorylation is a marker of progression of human liver disease. Hepatology 2004;40:459–466.
15. Ku NO, Omary MB. A disease- and phosphorylation-related nonmechanical function for keratin 8. J Cell Biol 2006;174:115–125.
16. Omary MB, Ku NO, Tao GZ, et al. 'Heads and tails' of intermediate filament phosphorylation: multiple sites and functional insights. Trends Biochem Sci 2006;31:383–394.
17. Ku NO, Soetikno RM, Omary MB. Keratin mutation in transgenic mice predisposes to Fas but not TNF-induced apoptosis and massive liver injury. Hepatology 2003;37:1006–1014.
18. Marceau N, Schutte B, Gilbert S, et al. Dual roles of intermediate filaments in apoptosis. Exp Cell Res 2007;313:2265–2281.
19. Denk H, Stumptner C, Zatloukal K. Mallory bodies revisited. J Hepatol 2000;32:689–702.
20. Zatloukal K, French SW, Stumptner C, et al. From Mallory to Mallory-Denk bodies: what, how and why? Exp Cell Res 2007;313:2033–2049.
21. Hanada S, Strnad P, Brunt EM, et al. The genetic background modulates susceptibility to mouse liver Mallory-Denk body formation and liver injury. Hepatology 2008;48:943–952.
22. Omary MB. 'IF-pathies': a broad spectrum of intermediate filament-associated diseases. J Clin Invest 2009;119:1756–1762.
23. Zatloukal K, Stumptner C, Lehner M, et al. Cytokeratin 8 protects from hepatotoxicity, and its ratio to cytokeratin 18 determines the ability of hepatocytes to form Mallory bodies. Am J Pathol 2000;156:1263–1274.
24. Strnad P, Zatloukal K, Stumptner C, et al. Mallory-Denk-bodies: lessons from keratin-containing hepatic inclusion bodies. Biochim Biophys Acta 2008;1782:764–774.
25. Stumptner C, Fuchsbichler A, Zatloukal K, et al. In vitro production of Mallory bodies and intracellular hyaline bodies: the central role of sequestosome 1/p62. Hepatology 2007;46:851–860.
26. Stumptner C, Fuchsbichler A, Heid H, et al. Mallory body–a disease-associated type of sequestosome. Hepatology 2002;35:1053–1062.
27. Fickert P, Trauner M, Fuchsbichler A, et al. Bile acid-induced Mallory body formation in drug-primed mouse liver. Am J Pathol 2002;161:2019–2026.
28. Brunt EM, Janney CG, Di Bisceglie AM, et al. Nonalcoholic steatohepatitis: a proposal for grading and staging the histological lesions. Am J Gastroenterol 1999;94:2467–2474.
29. Toivola DM, Nieminen MI, Hesse M, et al. Disturbances in hepatic cell-cycle regulation in mice with assembly-deficient keratins 8/18. Hepatology 2001;34:1174–1183.
30. Rangaswami H, Bulbule A, Kundu GC. Osteopontin: role in cell signaling and cancer progression. Trends Cell Biol 2006;16:79–87.
31. Lorena D, Darby IA, Gadeau AP, et al. Osteopontin expression in normal and fibrotic liver. Altered liver healing in osteopontin-deficient mice. J Hepatol 2006;44:383–390.
32. Rangaswami H, Bulbule A, Kundu GC. Nuclear factor inducing kinase: a key regulator in osteopontin- induced MAPK/IkappaB kinase

dependent NF-kappaB-mediated promatrix metalloproteinase-9 activation. Glycoconj J 2006;23:221–232.

33. Lee SH, Seo GS, Park YN, *et al.* Effects and regulation of osteopontin in rat hepatic stellate cells. Biochem Pharmacol 2004;68:2367–2378.

34. Pallari HM, Eriksson JE. Intermediate filaments as signaling platforms. Sci STKE 2006;2006:pe53.

35. Magin TM, Schroder R, Leitgeb S, *et al.* Lessons from keratin 18 knockout mice: formation of novel keratin filaments, secondary loss of keratin 7 and accumulation of liver-specific keratin 8-positive aggregates. J Cell Biol 1998;140:1441–1451.

36. Nakamichi I, Toivola DM, Strnad P, *et al.* Keratin 8 overexpression promotes mouse Mallory body formation. J Cell Biol 2005;171:931–937.

37. Harada M, Strnad P, Resurreccion EZ, *et al.* Keratin 18 overexpression but not phosphorylation or filament organization blocks mouse Mallory body formation. Hepatology 2007;45:88–96.

38. Mahajan V, Klingstedt T, Simon R, *et al.* Cross beta-sheet conformation of keratin 8 is a specific feature of Mallory-Denk bodies compared to other hepatocyte inclusions. Gastroenterology 2011;141:1080–1090. e1-7.

39. Moscat J, Diaz-Meco MT. p62 at the crossroads of autophagy, apoptosis, and cancer. Cell 2009;137:1001–1004.

40. Nan L, Wu Y, Bardag-Gorce F, *et al.* p62 is involved in the mechanism of Mallory body formation. Exp Mol Pathol 2004;77:168–175.

41. Strnad P, Harada M, Siegel M, *et al.* Transglutaminase 2 regulates Mallory body inclusion formation and injury-associated liver enlargement. Gastroenterology 2007;132:1515–1526.

42. Moscat J, Diaz-Meco MT. To aggregate or not to aggregate? A new role for p62. EMBO Rep 2009;10:804.

43. Ku NO, Gish R, Wright TL, *et al.* Keratin 8 mutations in patients with cryptogenic liver disease. N Engl J Med 2001;344:1580–1587.

44. Fickert P, Stoger U, Fuchsbichler A, *et al.* A new xenobiotic-induced mouse model of sclerosing cholangitis and biliary fibrosis. Am J Pathol 2007;171:525–536.

45. Syn WK, Choi SS, Liaskou E, *et al.* Osteopontin is induced by hedgehog pathway activation and promotes fibrosis progression in nonalcoholic steatohepatitis. Hepatology 2011;53:106–115.

46. Desmet VJ, van Eyken P, Roskams T. Histopathology of vanishing bile duct diseases. Adv Clin Path 1998;2:87–99.

47. Zollner G, Wagner M, Fickert P, *et al.* Expression of bile acid synthesis and detoxification enzymes and the alternative bile acid efflux pump MRP4 in patients with primary biliary cirrhosis. Liver Int 2007;27: 920–929.